The Williams syndrome chromosome 7q11.23 hemideletion confers hypersocial, anxious personality coupled with altered insula structure and function

Mbemba Jabbi[a,b,1,2], J. Shane Kippenhan[a,b,1], Philip Kohn[a,b], Stefano Marenco[b], Carolyn B. Mervis[c], Colleen A. Morris[d], Andreas Meyer-Lindenberg[a,b,3], and Karen Faith Berman[a,b,2]

[a]Section on Integrative Neuroimaging, National Institute of Mental Health, Intramural Research Program, National Institutes of Health, Bethesda, MD 20892; [b]Clinical Brain Disorders Branch, Genes, Cognition and Psychosis Program, National Institute of Mental Health, Intramural Research Program, National Institutes of Health, Bethesda, MD 20892; [c]Neurodevelopmental Sciences Laboratory, Department of Psychological and Brain Sciences, University of Louisville, Louisville, KY 40208; and [d]Department of Pediatrics, University of Nevada School of Medicine, Las Vegas, NV 89128

Edited* by Mortimer Mishkin, National Institute for Mental Health, Bethesda, MD, and approved February 2, 2012 (received for review September 20, 2011)

Although it is widely accepted that genes can influence complex behavioral traits such as human temperament, the underlying neurogenetic mechanisms remain unclear. Williams syndrome (WS), a rare disorder caused by a hemizygous deletion on chromosome 7q11.23, including genes important for neuronal migration and maturation (*LIMK1* and *CLIP2*), is typified by a remarkable hypersocial but anxious personality and offers a unique opportunity to investigate this open issue. Based on the documented role of the insula in mediating emotional response tendencies and personality, we used multimodal imaging to characterize this region in WS and found convergent anomalies: an overall decrease in dorsal anterior insula (AI) gray-matter volume along with locally increased volume in the right ventral AI; compromised white-matter integrity of the uncinate fasciculus connecting the insula with the amygdala and orbitofrontal cortex; altered regional cerebral blood flow in a pattern reminiscent of the observed gray-matter alterations (i.e., widespread reductions in dorsal AI accompanied by locally increased regional cerebral blood flow in the right ventral AI); and disturbed neurofunctional interactions between the AI and limbic regions. Moreover, these genetically determined alterations of AI structure and function predicted the degree to which the atypical WS personality profile was expressed in participants with the syndrome. The AI's rich anatomical connectivity, its transmodal properties, and its involvement in the behaviors affected in WS make the observed genetically determined insular circuitry perturbations and their association with WS personality a striking demonstration of the means by which neural systems can serve as the interface between genetic variability and alterations in complex behavioral traits.

brain | genetics | copy number variant | MRI | PET

The human insula, particularly its anterior portion, engenders awareness by integrating cognitive, interoceptive, and affective information (1–4). This brain region has been implicated in the mediation of subjective feeling states (1–4), prediction of aversive outcomes (5), empathy for both noxious (6, 7) and pleasant (7) emotional states, and the capacity to understand and simulate mental states of others (4, 8). Structural and functional alterations of the anterior insula (AI) complex, including the frontal operculum, are associated with impaired awareness of cognitive, affective, and social processes and can be manifested in unstable personality and other neuropsychiatric conditions (4, 9, 10). However, little is known about the genetic underpinnings of this region's neurobiology and whether any such genetically determined neural features might mediate behavioral responses and temperament.

Of particular interest to this line of investigation, Williams syndrome (WS), a rare genetic disorder [~1 in 7,500 live births (11)], is typified not only by impaired visuospatial construction abilities but also by strikingly unusual and distinctive personality traits, including hypersociability, increased empathy, and anxiety (12–14). The WS personality profile (WSPP) (15), based on ratings on the people-oriented, gregarious, visible, sensitive, and tense items on the Multidimensional Personality Questionnaire (MPQ) (16), quantitatively integrates several of the unusual characteristics of individuals with this syndrome (15, 16). This empirically derived personality profile measure correctly classifies individuals with WS with 96% sensitivity and differentiates them from a mixed-etiology developmental disabilities group with 85% specificity (15). The existence of this well delineated WSPP, along with the known genetic architecture of WS, offers unique opportunities to investigate the neurogenetic basis of higher-order human qualities, particularly social functioning and anxiety (12–15, 17, 18), with which the insula has been associated (1–10, 18).

WS is caused by a well documented 1.6-Mb hemizygous deletion of approximately 25 genes on chromosome 7q11.23 (19), a number of which likely interact to produce the brain and behavioral features of WS. Several of these genes have been studied in KO mice and have been found to play an important role in neurodevelopment, including the *LIM domain kinase 1* (*LIMK1*) (20) and *cytoplasmic linker protein 2* (*CLIP2*) (21) genes, both involved in neuronal migration/maturation, and a general transcription factor gene (*GTF2IRD1*) implicated in altered serotonin metabolism (22). These mouse studies also documented alterations in fear response [for both *LIMK1* and *GTF2IRD1* (20,22)] and reduced aggression [for *GTF2IRD1* (22)]. In parallel with these preclinical observations, research on the neural mechanisms underlying WS-specific behavioral characteristics has identified functional and structural alterations of the intraparietal sulcus (12, 23–26), hippocampal formation (27), amygdala, and orbitofrontal cortex (OFC) (12, 17, 28), and aberrant orbitofrontal circuitry has been associated with the syndrome's distinctive pattern of emotional processing: remarkable lack of social fear coupled with a high incidence of nonsocial anxieties and phobias (17, 29, 30).

Several lines of evidence link the insula to the amygdala-OFC circuit found to be aberrant in WS (12, 17, 28). These structures,

Author contributions: M.J. and K.F.B. designed research; M.J., J.S.K., P.K., S.M., C.B.M., A.M.-L., and K.F.B. performed research; C.B.M. and C.A.M. recruited and managed participants; M.J., J.S.K., P.K., S.M., and C.B.M. analyzed data; and M.J., J.S.K., S.M., C.B.M., A.M.-L., and K.F.B. wrote the paper.

The authors declare no conflict of interest.

*This Direct Submission article had a prearranged editor.

[1]M.J. and J.S.K. contributed equally to this work.

[2]To whom correspondence may be addressed. E-mail: karen.berman@nih.gov or jabbim@gmail.com.

[3]Present address: Central Institute of Mental Health, D-68159 Mannheim, Germany.

See Author Summary on page 5164 (volume 109, number 14).

This article contains supporting information online at www.pnas.org/lookup/suppl/doi:10.1073/pnas.1114774109/-/DCSupplemental.

along with anterior cingulate cortex (ACC), jointly integrate physiological arousal states with cognitive processes during valuation and emotion processing (1–10, 31). Of relevance to the altered fronto-amygdalar responses and connectivity during affect processing in WS (12, 17, 28, 30), the insula is anatomically interconnected with subregions of the amygdala, OFC, and ACC (32–34). Moreover, the AI is cytoarchitectonically characterized by marked abundance of von Economo neurons (35), which are also selectively present elsewhere in the so-called "salience network" (36), including the OFC and ACC, of humans and nonhuman primates (37); these neurons may play an important role in regulating executive control relevant for emotional awareness (4, 35, 37, 38). These findings, together with reports of structural perturbations of the AI (39), suggest that the human insula, especially the AI, is a neural target through which the genetically determined atypical empathy, nonsocial anxiety, and hypersocial WS personality (12–15, 29) may be mediated. The insula's integral role in both the brain circuits and behaviors that are prominently affected in WS formed the basis of our hypothesis-driven investigation of this region in WS.

Specifically, we hypothesized that structure, function, and connectivity of the insula would be altered in WS and that these genetically determined alterations would be related to the WSPP. To test this hypothesis, we measured gray-matter volume and white-matter connectivity with MRI and diffusion tensor imaging (DTI), respectively, as well as regional cerebral blood flow (rCBF) and functional connectivity with PET, and we investigated whether these brain measures predicted the degree to which the WS personality traits (15) were present in individual participants with WS.

Results

Altered Insula Gray-Matter Volume. For the manually delineated volumes of interest (VOIs; Fig. 1*A*), gray-matter volume of the insula as a whole was significantly decreased in WS relative to controls [$F_{(1,35)} = 12.85$; $P = 0.001$]. This result was also observed [$F_{(1,35)} = 5.52$; $P = 0.025$] when insula volume was considered as a ratio of total cerebral volume [total cerebral volume, as expected (40) was significantly decreased in WS: $F_{(1,35)} = 6.001$; $P = 0.019$]. Post-hoc analyses revealed that gray-matter volume was reduced in WS for the right insula as a whole [$F_{(1,35)} = 7.36$; $P = 0.01$], as well as for both left and right AIs [$F_{(1,35} = 7.37$, $P = 0.01$; and $F_{(1,35)} = 5.36$; $P = 0.027$, respectively; Fig. 1*B* and Table S1].

Our DARTEL-guided voxel-based morphometry (VBM) analyses (*Methods*) allowed more detailed localization of gray-matter alterations, and showed extensive reductions in bilateral insula gray-matter volume in WS. These reductions were most robust in the right and left AI [$t = 6.19$, $P = 0.0005$ and $t = 5.80$, $P = 0.0005$, respectively, false discovery rate (FDR)-corrected for whole brain; Table S2]. When accounting for variation in whole-brain volume, we found decreased gray-matter volume in WS in the right dorsal AI, extending to the frontal operculum and striatum ($t = 3.80$, $P = 0.019$, FDR), as well as in the left dorsal AI ($t = 4.35$, $P = 0.007$, FDR; Fig. 1*C* and Table S3). Clusters of reduced gray-matter volume were also observed in the left and right middle insula ($t = 3.92$, $P = 0.013$; and $t = 3.88$, $P = 0.014$, FDR). In contrast, this analysis also revealed a localized area of increased gray-matter volume in the right ventral AI (vAI) extending to the frontal operculum/OFC in the WS group ($t = 4.60$, $P = 0.001$, FDR; Fig. 1*C* and Table S3). These convergent VOI and VBM findings of bilaterally reduced dorsal AI volume, along with locally increased gray-matter volume in the right vAI/OFC in the WS group relative to carefully matched controls, strongly suggest the existence of genetically determined structural alterations of the AI that may have functional repercussions and also be manifested in altered connectivity of the AI with other brain regions.

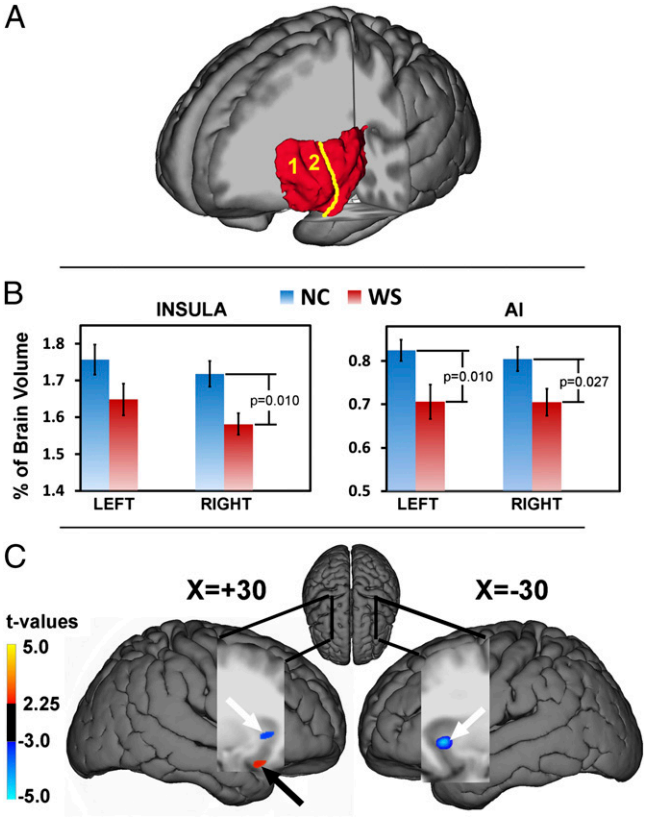

Fig. 1. Structural alteration of the insula in WS. (*A*) Sample image of a manually segmented left insula (red structure) of a healthy control participant. The yellow line indicates the approximate demarcation between the AI (consisting of the accessory "1" and anterior short "2" gyri) and mid-posterior insula. (*B*) Bar graphs, including error bars depicting SEM, show reduced volume of the right insula as a whole and the AI bilaterally in WS. (*C*) VBM findings of reduced bilateral AI gray-matter volume in WS relative to controls (blue clusters with white arrows) with the local maxima located in the Montreal Neurological Institute coordinates *x*, *y*, and *z* of 30, 20, and 0 (right AI) and −30, 19, −3 (left AI), respectively. We also found increased gray-matter volume in WS (red cluster with black arrow) in the right vAI: *x*, *y*, and *z* of 30, 14, and −22, respectively. Statistical maps (*t* value color scale) are overlaid onto a group-specific DARTEL-normalized T1 structural template. Tables S1–S3 provide complete lists of structural results.

Altered Structural Connectivity of AI via Uncinate Fasciculus. In the left uncinate fasciculus (connecting AI, amygdala, and OFC), we found significant reductions of fractional anisotropy (FA) (41) in WS ($z = 2.40$, $P = 0.015$, two-tailed Mann–Whitney *U* test; Fig. 2 *A*–*C*), providing direct evidence of altered AI connectivity at the anatomical level, consistent with the aberrant OFC-amygdala functional connectivity that has been reported in WS (17) as well as with our functional connectivity findings (as detailed later). Results of between-group comparison of FA in the right uncinate fasciculus did not reach statistical significance, perhaps reflecting the observed increase in right vAI gray-matter volume in the WS group.

Altered Resting rCBF of Insula. rCBF was reduced in the WS group in the right dorsal middle/posterior insula ($t = 6.74$; $P = 0.005$ FDR, two-sample *t* test; SPM5 software package), the left dorsal AI ($t = 3.00$; $P = 0.032$ FDR), and the midportion of the insula ($t = 5.92$; $P = 0.005$ FDR), as well as in the hippocampal formation/amygdala bilaterally (Fig. 3 *A* and *B* and Table S4). In contrast, a ventral portion of the right AI and OFC showed increased resting rCBF in the WS group ($t = 4.92$; $P = 0.021$ FDR), localized to the same region where gray-matter volume

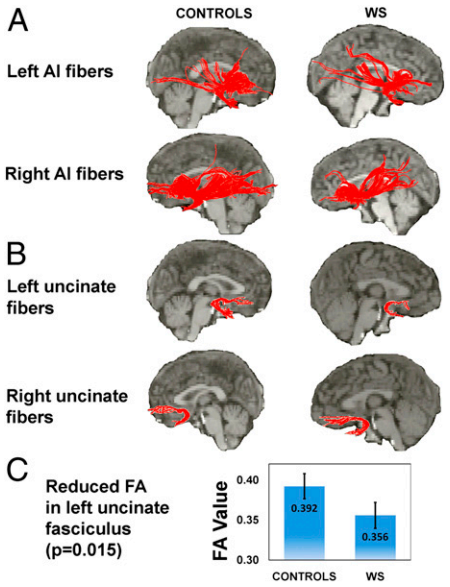

Fig. 2. AI white-matter and specific uncinate fasciculus tractography maps. (*A*) Tractographic maps of the left and right AI of the median control participant and median WS participant; fiber tracts for each individual participant are shown superimposed on the median participants' anatomical images. (*B*) Separate VOI-generated fiber pathways of the left and right uncinate fasciculus of the same individuals. (*C*) Significant reductions in FA values in the left uncinate fasciculus ($z = 2.40$, $P = 0.015$, two-tailed Mann–Whitney *U* test). Error bars indicate SEM.

was increased in WS (Fig. 3*C* and Table S4). Nearby OFC regions also exhibited this increased rCBF (Fig. 3*C*).

Altered Resting Functional Connectivity of Insula. Brain areas in which there were between-group differences in correlations of AI rCBF with rCBF in other regions are detailed in Table S5. Maps of these regions as well as graphical representations of the underlying within-group interregional relationships are shown in Fig. 4. In the control group, rCBF of both left and right AI was positively coupled with a network including ACC, OFC, the posterior insula, and the amygdala, whereas a negative relation was observed between AI and middorsal cingulate.

The direct voxel-wise statistical comparison between AI functional connectivity maps of the controls and the WS participants revealed that the interregional relations observed in the controls were absent or became negative in the WS group (Fig. 4 *A–F* and Table S5). These altered AI resting rCBF couplings in WS were found predominantly in the anatomically interconnected (32–34) salience network (36), in line with our findings of anomalous gray and white matter integrity in this system reported here, as well as with previous findings of perturbations in OFC-amygdala coupling during processing of social emotions (17).

Altered AI Structure and Function Predict WS Personality. By examining the relation between these genetically driven AI alterations and WSPP scores, we identified a positive correlation between the degree to which the characteristic WS personality was expressed in the WS individuals and gray-matter increase in the right vAI ($z = 2.42$; $P = 0.008$, whole-brain uncorrected; Fig. 5*B*), localized to a region where gray-matter volume in the WS group had been found to be increased relative to the control group (Fig. 1*C*).

Similarly, to assess the relation between insula function and personality traits in participants with WS, we used the same statistical approach and found a positive correlation between WSPP scores and resting rCBF in the right vAI ($z = 5.10$; $P = 0.0001$, uncorrected; Fig. 5*C*), again localized to the region where rCBF was abnormally increased in the WS group (Fig. 3*C*). In addition, functional and structural alterations in several other regions including the superior temporal cortex (STS) and the temporoparietal junction (TPJ) also correlated with WSPP (Table 1).

To assess the specificity of the observed structural and functional correlations of WSPP with vAI and its connected pathway, we examined the relationship between WSPP and PET/VBM measures within the anterior hippocampus [a region where structure, function, and metabolism have previously been shown to be significantly altered in WS (27), and that is additionally implicated in LIMK1 and CLIP2 KO mouse models (20,21)], and found no correlations between these measures even at a liberal statistical threshold of $P < 0.01$ uncorrected. We additionally performed similar analyses with another behavioral measure that is not based on personality (the Verbal IQ score on the Wechsler Abbreviated Scale of Intelligence). We found no significant correlations (at $P < 0.01$, uncorrected) within the insula or in any of the other related regions for this measure.

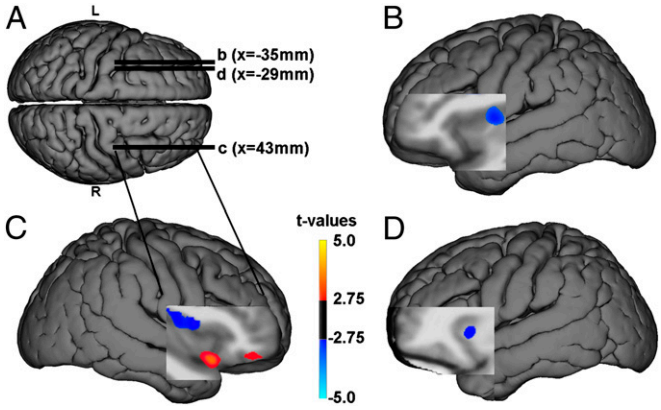

Fig. 3. Resting rCBF differences in WS relative to controls. Blue clusters indicate reduced rCBF in WS, whereas orange indicates increased rCBF in WS. (*A*) Superior view of group-specific DARTEL-normalized T1 structural surface shows sagittal slice positioning in *B–D*. (*B* and *D*) Decreased rCBF in WS: left dorsal midanterior (*B*) and anterior (*D*) insula. (*C*) Blue indicates decreased rCBF in WS in dorsal mid-AI; orange indicates increased rCBF in WS in right vAI and OFC. Table S4 shows stereotaxic coordinates and a complete list of results.

Discussion

Our multimodal approach afforded a detailed description of the genetically driven characteristics of the WS insula and yielded convergent findings of (*i*) altered insula gray-matter volume centered in the AI, (*ii*) compromised white-matter integrity of the left uncinate fasciculus connecting the AI with the amygdala and OFC, (*iii*) altered resting rCBF in the AI, and (*iv*) anomalous functional connectivity of the AI. These data suggest the existence of a genetically determined, insula-based mechanism that may underlie the unique behavioral phenotype of atypical temperament and social functioning in WS. Notably, the latter point is supported not only by the insula's known involvement in the personality traits that distinguish individuals with WS, but also more specifically by our finding that functional and structural alterations of the AI predicted a well validated sensitive and specific measure of the hypersocial, anxious, and empathic WS personality.

Manual delineation of insula gray-matter volume demonstrated a reduction of the right insula as a whole, as well as of the AI portion bilaterally, in individuals with WS. VBM analyses revealed additional anomalous features at the subregional level: extensive gray-matter reduction in dorsal AI as well as a localized increase in vAI. In line with these gray-matter findings, we also detected compromised white-matter integrity (i.e., reduced

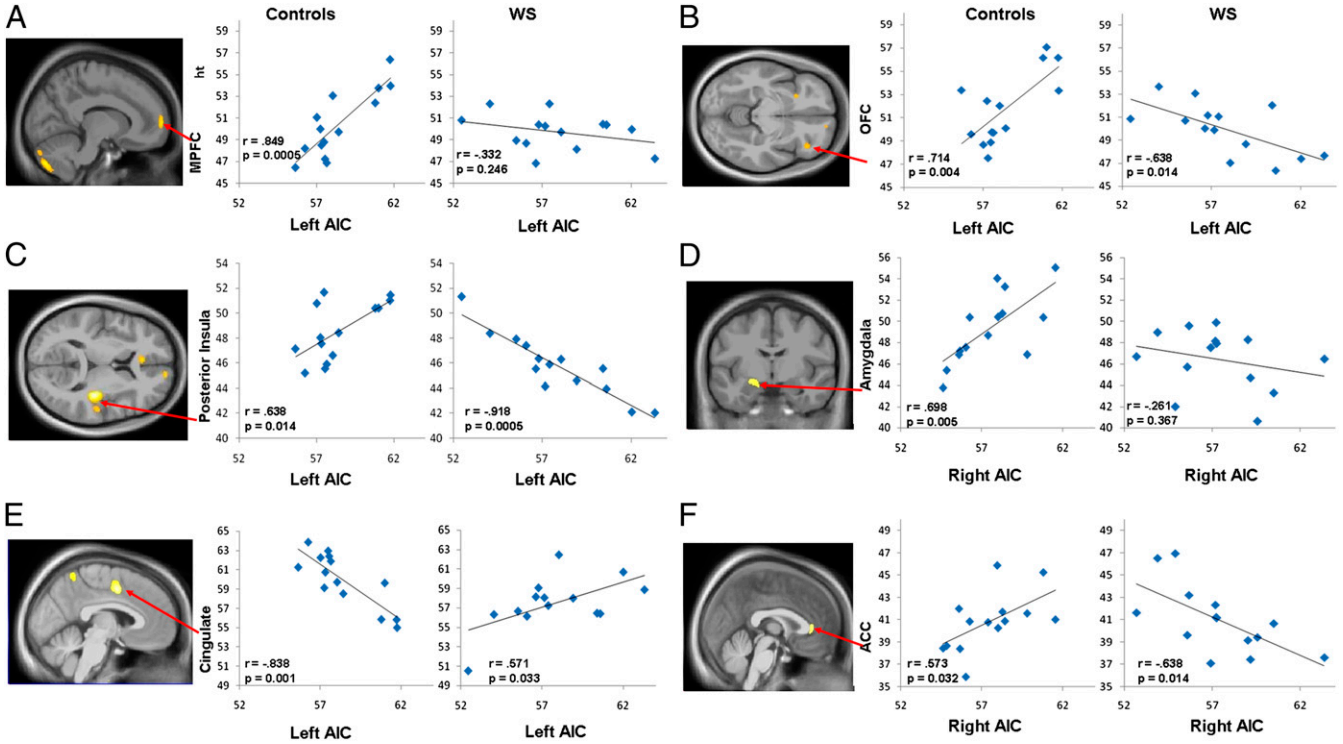

Fig. 4. Altered functional rCBF connectivity of left AI (*A–C*) and right AI (*D–F*) in WS and healthy controls. Maps show between-group voxel-wise comparisons of AI connectivity displayed at $P < 0.005$ uncorrected and superimposed on average DARTEL normalized group sagittal, coronal, and axial anatomical images (Table S4). Graphs show within-group Pearson correlation coefficients. AIC, anterior insula cortex.

FA) in the left uncinate fasciculus. Given the role of the uncinate fasciculus in relaying synaptic information between the fronto-amygdalar system and the AI (26–28), this compromised amygdala-OFC white-matter connectivity via the AI, along with our findings of negative functional rCBF coupling of right vAI with OFC and dorsal insular subregions, provides direct anatomical and functional support for previous findings of disrupted functional fronto-amygdala connectivity in WS during processing of emotions (17, 28). These results are consistent with neuroanatomical evidence suggesting marked rightward asymmetry of this system in normal subjects (35, 42). Thus, the enlarged vAI on the right side and the preservation of normal FA in the right uncinate fasciculus in WS may be related to the prevalence of von Economo neurons in the right AI (35) and a preponderance of uncinate fasciculus volume and fiber numbers on the right side in normal subjects (42).

The resting rCBF analyses demonstrated reduced blood flow in dorsal AI, as well as increases in right vAI, in participants with WS. Overall, our VBM and rCBF analyses revealed remarkably convergent subregional patterns of alteration: gray-matter reductions in dorsal AI were accompanied by rCBF reductions in the same area; likewise, gray-matter increases in right vAI were accompanied by local increases in rCBF. These multimodal findings were echoed behaviorally by the demonstration that, the more abnormally increased the vAI rCBF and gray-matter volume, the more the WS personality was expressed in a given participant with WS.

The localization of structural and functional correlates of the WS personality to the right vAI (here shown to be structurally and functionally increased in WS) is particularly interesting in light of a meta-analysis of 1,768 human functional neuroimaging experiments, which identified this ventral portion of the insula as functionally distinctive regarding its particular involvement in human social emotional processes; in contrast, the dorsal AI (here shown to be reduced in gray-matter volume and resting rCBF in WS) was more associated with affective-cognitive integration by this meta-analysis (43). Thus, our findings, along with the known involvement of the insula and related circuitry in interoception, emotional regulation (1–7, 43), and affiliative behavior (44), suggest a genetically determined role for this network of regions in regulating complex behavioral traits such as social response tendencies.

In addition, both gray-matter volume and resting rCBF in cingulate, OFC, STS, and TPJ were related to the distinctive WS personality (Table 1). That these latter regions predict WS personality is of interest because the STS and TPJ have been implicated in the attribution of agency and in theory of mind (46), aspects of which are shown to be aberrant in WS (refs. 46, 47, but see ref. 48). Together, these findings suggest the involvement of a broader network of regions [localized predominantly in the social brain pathways (45)] in the WS behavioral profile than previously appreciated, offering potential neurogenetic insight into other conditions with a heritable component and atypical personality and social function. Of particular interest to our observations that vAI volume and function predict the WSPP, a recent meta-analysis of neuroimaging studies of social function in autism (49) observed a locus of decreased activation in a right AI region similar to that delineated by our work. Together, these results suggest a complex involvement of the AI region and connected pathways in social behavior.

The data regarding task-independent, resting rCBF-based functional connectivity, a measure that is emerging as an important marker of the integrity of intrinsic neuronal pathways (50), demonstrated altered cooperativity between key regions in WS, namely reduced correlations between rCBF in both left and right AI and rCBF in regions within a neural circuit including ACC, OFC, and amygdala that is associated with salience processing (36, 38). Specifically, this functional coupling was predominantly positive in controls but absent or negative in the participants with WS. These results further highlight disturbances

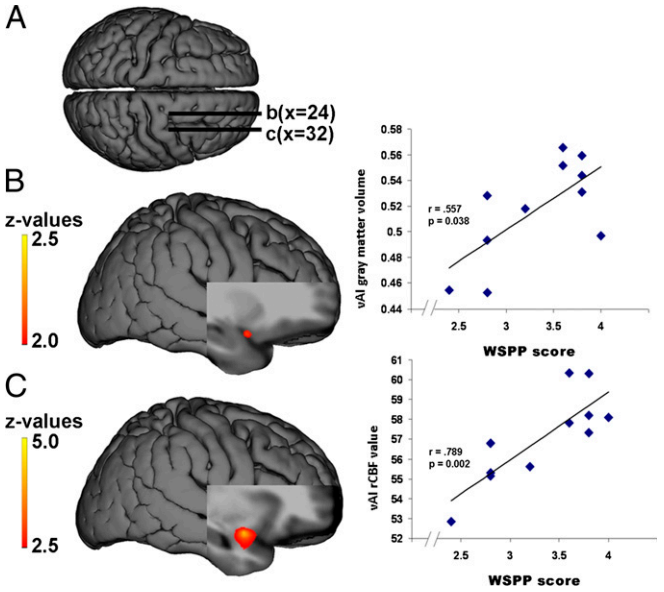

Fig. 5. Neural correlates of the WSPP (15). (*A*) Superior view of group-specific DARTEL-normalized T1 structural surface shows sagittal slice positioning in *B* and *C*. (*B*) Statistical map of correlations between scores on the WSPP measure and gray-matter volume in right vAI, along with scatter plot at *x*, *y*, and *z* of 33, 15, and −25, respectively. (*C*) Correlation map of WSPP and rCBF in ventral right AI, alongside the scatter plot at *x*, *y*, and *z* of 31, 6, and −18, respectively. Color bars represent *z* values of the gray-matter and rCBF correlation maps, shown on the DARTEL-normalized group-average anatomical images. Spearman ρ nonparametric correlation coefficients are given in the graphs. Table 1 shows a complete list of correlated clusters.

Table 1. Neural correlates of WSPP

Anatomical description	MNI coordinate X	Y	Z	*z* value	*P* value
Gray-matter volume					
AI (ventral)	33	15	−24	2.42	0.008*
AI/OFC (ventral)	24	8	−20	2.26	0.012
Medial OFC	15	31	−24	4.46	0.0001
Medial prefrontal cortex	−10	58	7	2.08	0.019
Posterior cingulate	−1	−40	17	3.21	0.001
Intraparietal sulcus	−21	−81	43	3.1	0.001
STS	−58	−34	0	2.83	0.002
TPJ	−47	−59	16	2.06	0.02
rCBF					
AI (ventral)	31	6	−18	5.10	0.0001*
AI/frontal operculum	32	36	4	2.79	0.003
Medial OFC	5	55	−20	3.63	0.0003
Anterior cingulate/medial prefrontal	−12	54	7	4.1	0.0001
Lateral OFC	−42	42	−4	3.42	0.0006
Medial temporal gyrus/amygdala	−26	3	−36	3.65	0.0003
Posterior cingulate	11	−46	50	3.65	0.0003
Superior frontal cortex	16	64	25	−3.28	0.001
Pons/brainstem	0	−18	−39	−3.35	0.0008
TPJ/STS	−58	−49	8	4.04	0.0001
TPJ	−54	−50	9	3.56	0.0004
STS	47	−29	2	3.12	0.001

Positive *z* values indicate a direct relationship; negative *z* values indicate an inverse relationship.
*AI correlations with WSPP (Fig. 5).

in a network of regions (17, 28) relevant for the processing of emotionally salient and arousing information (38).

With our finding of altered AI structure, function, and connectivity, this brain region joins the list of transmodal cortical regions already implicated in WS. These include the hippocampal formation, IPL, amygdala, and OFC (12, 14, 17, 20, 23–28, 30). Such transmodal cortical systems (51) are composed of subregionally specialized and highly interconnected heteromodal, paralimbic, and limbic cortices (51–53). These nodes bind multiple unimodal and other transmodal areas into distributed but integrated multimodal representations and are therefore critically important for cortical/subcortical information flow (4, 51–53). Because transmodal cortical areas, such as the AI, provide a nexus for interregionally coordinated neural activity and have particularly rich anatomical and functional connections, they may be especially vulnerable to aberration in the expression of genes that are crucial for successful neuronal migration and maturation like *LIMK1* (20) and *CLIP2* (21), which are hemideleted in WS (19–21). Such vulnerabilities may lead to malformations in transmodal nodes, and their connections, during critical developmental periods of cortical organization. Our present findings of alterations in the uncinate fasciculus, along with previous demonstrations of abnormalities in white-matter tracts connecting other transmodal regions in WS (25, 26), provide support for this proposed neurogenetic mechanism.

Several points regarding our findings deserve comment. First, the majority of individuals with WS have mild to moderate intellectual impairment, and their ability to cooperate with complex neuroimaging procedures can be limited. Although important information about WS has been obtained by studying such individuals, for the multimodal imaging studies reported here, we searched for extremely rare persons with WS and normal IQs, who nonetheless have the same visuospatial construction impairment and hypersocial personality that characterize the syndrome, along with genetically confirmed typical hemideletions in the WS critical region of chromosome 7. We chose this approach not only to maximize the participants' ability to cooperate with the procedures and hence the quality of the imaging data, but also because the alternative strategy of comparing intellectually impaired individuals with WS to a normal intelligence control group can present a potential confound in the interpretation of the neuroimaging data, as group differences could be related to low IQ per se. Indeed, we previously reported (25) a relationship between DTI measures and IQ in WS, highlighting the importance of selecting diagnostic groups matched by IQ, as we did here. Moreover, abnormalities found in our high-functioning group are likely to also be present in individuals with WS with intellectual impairment [as has been demonstrated in previous studies (26, 28, 54)], but nonspecific aspects of brain structure and function associated with intellectual impairment will not be represented in our cohort. Therefore, the neurobiological phenotype reported here is likely to be proximal to the genetic substrate of the disorder, rather than to intellectual impairment per se, consistent with our overall objective of using neuroimaging to forge a link between the effects of specific genes and brain mechanisms of cognitive and behavioral disorders.

A second important point is that, although growing evidence suggests that the genesis of the atypical WS personality rests in aberrant neural structure and function of the WS brain, it is also possible that experiences and behaviors may impact neuroplasticity of the developing brain (54, 55), as well as personality measures. Therefore, longitudinal studies that track the trajectory of neural growth, in association with behavioral features, in children with WS may help clarify whether the neuroanatomical features characterized in adults are present from birth or impacted by developmental and environmental factors (55, 56). The empirical relationship we report between WSPP scores and neuroimaging data are specifically based on our cohort. Additional studies will be necessary to determine whether the observed correlation between

WSPP scores and ventral-AI structure and function extends to the larger WS population across the entire age span.

In sum, the anatomically special position of the AI, particularly its well documented structural (32–34) and functional interconnectivity (57) with the salience circuit and related networks, along with its strong functional involvement in the behaviors (1–8, 58, 59) affected in WS, make the observed insular circuitry perturbations and their association with the distinctive WS personality a striking illustration of how neural systems serve as the interface between genetic variability and alterations in complex behavioral traits. The present observations, in a rare population of individuals with well known genetic architecture and unique personality features, not only provide a deeper understanding of WS, but also inform the search for neural mechanisms by which genetic features contribute to complex behavior (60), both in the general population and in neuropsychiatric disorders.

Methods

Participants. As outlined previously (17, 23), the WS participants all had IQs within the normal range and were in good physical health. Healthy controls (free of neurological and/or psychiatric diagnosis) were matched for IQ, sex, and age with the WS group (Table 2). Thirty-seven participants (14 with WS, seven female; 23 healthy controls, 10 female) participated in structural MRI scanning; 14 control subjects (five female) from the larger cohort and all 14 participants with WS underwent PET scanning. Five participants with WS (one female) completed DTI scans and were matched pairwise with five control participants for age, sex, and IQ (25). Parents of 11 participants with WS completed the parent report form of the MPQ (16). Most of the rare WS cohort also participated in previously reported studies. All participants were right-handed, and all gave written informed consent according to National Institutes of Health Institutional Review Board guidelines.

Structural MRI Acquisition and Analysis. By using six axially acquired, intensity-normalized, registered, and averaged T1-weighted 1.5 T structural MRIs ($0.9375 \times 0.9375 \times 1.2$ mm; GE) (23) for each participant, we assessed structural integrity of insular gray matter in two ways: a volume-of-interest (VOI) and a voxel-wise approach. First, for the VOI analysis, an operator blinded to diagnostic information manually delineated each individual's insulae in native space, in line with Cohen et al. (39), using ITKSnap software (http://www.itksnap.org/). The AI was demarcated by segmenting the first two insular gyri (accessory and anterior short; Fig. 1*A*) in the axial plane, while simultaneously visualizing sagittal and coronal planes. Cross-group comparisons of whole-insula volumes were carried out with and without ratio normalization for brain size by using a mixed-model ANOVA with two factors (hemisphere and diagnosis, with hemisphere as a repeated measure).

Next, to more precisely localize gray-matter volume alterations, we performed VBM analyses (61) by using enhanced spatial alignment methods (DARTEL). T1 images were segmented, and gray-matter maps were used to iteratively derive a group-specific template and a set of individual diffeomorphic transformations that warped each participant's data to this specific template. Jacobian modulation accounted for local expansions or contractions of the diffeomorphic warp into standard space. DARTEL-normalized, Jacobian-modulated gray-matter maps were smoothed (8-mm full width at half maximum) and compared across groups first with an SPM5-based ANOVA, and then with analysis of covariance by using whole-brain volume covariates (27), both at $P < 0.05$ (FDR-corrected) for the whole brain.

DTI Acquisition and Analysis. To assess white-matter integrity, specifically the anatomical connectivity of the AI with the amygdala and OFC via the uncinate fasciculus, we used single-shot echo-planar imaging (six gradient directions with *b* value ~1,100 s/mm^2 plus one acquisition with *b* value ~0 s/mm^2, 2-mm isotropic resolution, echo time of 82.7 ms, repetition time >10 s, cardiac-gated, gradient strength 5 G/cm, eight repetitions) on a Signa 1.5-T scanner (GE) (25). DTI Studio software (41) was used to perform tractography as described earlier (25). We selected white-matter fibers immediately adjacent to the AI by creating an initial VOI based on the insula volumes that had been manually segmented on the structural MRIs, dilated each insula volume medially by 2 mm, and subtracted the original insula volume from the dilated volume, leaving a mask that included the capsula extrema (Fig. S1). This mask was then transformed into DTI space (25).

We then selected the set of fibers passing through the uncinate fasciculus by drawing a second VOI encompassing the temporal fibers emanating from the AI on the first coronal slice where the separation between frontal and temporal lobes became visible. Only those fibers occurring in the initial and the second VOIs were included (62), thus exclusively retaining fibers of the uncinate fasciculus. Mann–Whitney *U* testing (nonparametric) was used to assess group differences in uncinate fasciculus FA at $P < 0.05$.

Table 2. Demographics

Study	WS	Control
Structural MRI*		
No. of pts.	14	23
Sex		
Male	7	13
Female	7	10
Age (yrs)	27.82 ± 9.3	32.1 ± 7.8
IQ	90.85 ± 9.2	94.21 ± 8.1
DTI		
No. of pts.	5	5
Sex		
Male	4	4
Female	1	1
Age	27.6 ± 6.4	27.1 ± 7.9
IQ	87.2 ± 5.8	91.8 ± 4.14
PET rCBF		
No. of pts.	14	14
Sex		
Male	7	8
Female	7	6
Age	27.8 ± 9.3	32.6 ± 7.9
IQ	90.8 ± 9.2	95.3 ± 9.4
WS Personality		
No. of pts.	11	—
Sex		
Male	4	—
Female	7	—
Age	29.0 ± 10.7	—
IQ	91.4 ± 9.1	—

Values presented as mean ± SD where appropriate.
*All participants were Caucasian except for one African American control subject in the structural MRI experiment.

PET rCBF Acquisition and Analysis. We used the gold-standard ^{15}O water method to measure task-independent resting rCBF, an indicator of basal metabolic level, in 14 WS and 14 control participants. Four 60-s rCBF scans per participant (12 mCi/scan by i.v. bolus) were acquired on an Advance 3D PET scanner (GE), attenuation-corrected, and reconstructed (32 planes, 6.5 mm isotropic). After preprocessing, including background subtraction and across-scan registration (27), the four PET images for each individual were registered to his or her own structural MRI, proportionally scaled to a whole-brain mean, DARTEL-normalized (61) to a group-specific template derived from the 28 WS and control participants, and then averaged and smoothed (10 mm^3 full width at half maximum). We then compared groups by using a random-effects model in SPM5 ($P < 0.05$ FDR-corrected at the whole-brain level).

Functional Connectivity Analyses. To assess resting functional connectivity, we applied each person's manually segmented AI structural volumes to his or her rCBF PET scan in native space to extract average left and right AI rCBF values. Then, in standardized space, these AI rCBF values were entered as covariates to determine their correlations with rCBF in all other voxels throughout the brain for each group, and the slopes of these correlations were statistically compared across the two groups voxel by voxel. We limited this analysis to AI connectivity, as the most significant group-related rCBF measures were specific to this region. We used a general linear model in SPM5 to test the hypothesis that functional connectivity (rCBF correlations) between the AI and related regions are altered in WS relative to controls, assessed at the whole-brain level at $P < 0.001$.

Assessment of WS Personality and Association with Brain Structure and Function. To assess personality in the participants with WS, parents were asked to complete the short form of the MPQ (15, 16), and the WSPP composite score was calculated following Klein-Tasman and Mervis (15), based on

five character trait ratings: gregarious, people-oriented, tense, sensitive, and visible. High scores indicate a better fit to the WSPP than low scores. To test for the predicted association between WS personality traits and alterations of insula structure and function, the highly sensitive and specific WSPP scores (15), along with age, were used as covariates in two separate second-level general linear-model analyses of the VBM and rCBF data.

ACKNOWLEDGMENTS. The authors thank Rosanna Olsen, Aaron Bonner-Jackson, and Paul Koch for their contribution toward data collection and management of the experiments and Dwight Dickinson for comments. This research was supported by the Intramural Research Program of the National Institute of Mental Health, National Institutes of Health and by National Institute of Neurological Disorders and Stroke Grant R01 NS35102 (to C.B.M.).

1. Critchley HD, Mathias CJ, Dolan RJ (2001) Neuroanatomical basis for first- and second-order representations of bodily states. *Nat Neurosci* 4:207–212.
2. Damasio A (2003) Feelings of emotion and the self. *Ann N Y Acad Sci* 1001:253–261.
3. Critchley HD, Wiens S, Rotshtein P, Ohman A, Dolan RJ (2004) Neural systems supporting interoceptive awareness. *Nat Neurosci* 7:189–195.
4. Craig AD (2009) How do you feel—now? The anterior insula and human awareness. *Nat Rev Neurosci* 10:59–70.
5. Singer T, Critchley HD, Preuschoff K (2009) A common role of insula in feelings, empathy and uncertainty. *Trends Cogn Sci* 13:334–340.
6. Singer T, et al. (2004) Empathy for pain involves the affective but not sensory components of pain. *Science* 303:1157–1162.
7. Jabbi M, Swart M, Keysers C (2007) Empathy for positive and negative emotions in the gustatory cortex. *Neuroimage* 34:1744–1753.
8. Adolphs R (2009) The social brain: Neural basis of social knowledge. *Annu Rev Psychol* 60:693–716.
9. Feinstein JS, Stein MB, Paulus MP (2006) Anterior insula reactivity during certain decisions is associated with neuroticism. *Soc Cogn Affect Neurosci* 1:136–142.
10. King-Casas B, et al. (2008) The rupture and repair of cooperation in borderline personality disorder. *Science* 321:806–810.
11. Strømme P, Bjørnstad PG, Ramstad K (2002) Prevalence estimation of Williams syndrome. *J Child Neurol* 17:269–271.
12. Meyer-Lindenberg A, Mervis CB, Berman KF (2006) Neural mechanisms in Williams syndrome: A unique window to genetic influences on cognition and behaviour. *Nat Rev Neurosci* 7:380–393.
13. Mervis CB, Klein-Tasman BP (2000) Williams syndrome: Cognition, personality, and adaptive behavior. *Ment Retard Dev Disabil Res Rev* 6:148–158.
14. Bellugi U, Lichtenberger L, Mills D, Galaburda A, Korenberg JR (1999) Bridging cognition, the brain and molecular genetics: Evidence from Williams syndrome. *Trends Neurosci* 22:197–207.
15. Klein-Tasman BP, Mervis CB (2003) Distinctive personality characteristics of 8-, 9-, and 10-year-olds with Williams syndrome. *Dev Neuropsychol* 23:269–290.
16. Tellegen A (1985) Structures of mood and personality and their relevance to assessing anxiety, with an emphasis on self-report. *Anxiety and the Anxiety Disorders*, eds Tuma AH, Maser JD (Lawrence Erlbaum, Hillsdale, NJ), pp 681–716.
17. Meyer-Lindenberg A, et al. (2005) Neural correlates of genetically abnormal social cognition in Williams syndrome. *Nat Neurosci* 8:991–993.
18. Etkin A, Wager TD (2007) Functional neuroimaging of anxiety: A meta-analysis of emotional processing in PTSD, social anxiety disorder, and specific phobia. *Am J Psychiatry* 164:1476–1488.
19. Osborne LR, Mervis CB (2007) Rearrangements of the Williams-Beuren syndrome locus: Molecular basis and implications for speech and language development. *Expert Rev Mol Med* 9:1–16.
20. Meng Y, et al. (2002) Abnormal spine morphology and enhanced LTP in LIMK-1 knockout mice. *Neuron* 35:121–133.
21. Hoogenraad CC, et al. (2002) Targeted mutation of Cyln2 in the Williams syndrome critical region links CLIP-115 haploinsufficiency to neurodevelopmental abnormalities in mice. *Nat Genet* 32:116–127.
22. Young EJ, et al. (2008) Reduced fear and aggression and altered serotonin metabolism in Gtf2ird1-targeted mice. *Genes Brain Behav* 7:224–234.
23. Meyer-Lindenberg A, et al. (2004) Neural basis of genetically determined visuospatial construction deficit in Williams syndrome. *Neuron* 43:623–631.
24. Kippenhan JS, et al. (2005) Genetic contributions to human gyrification: Sulcal morphometry in Williams syndrome. *J Neurosci* 25:7840–7846.
25. Marenco S, et al. (2007) Genetic contributions to white matter architecture revealed by diffusion tensor imaging in Williams syndrome. *Proc Natl Acad Sci USA* 104: 15117–15122.
26. Hoeft F, et al. (2007) More is not always better: Increased fractional anisotropy of superior longitudinal fasciculus associated with poor visuospatial abilities in Williams syndrome. *J Neurosci* 27:11960–11965.
27. Meyer-Lindenberg A, et al. (2005) Functional, structural, and metabolic abnormalities of the hippocampal formation in Williams syndrome. *J Clin Invest* 115:1888–1895.
28. Haas BW, et al. (2009) Genetic influences on sociability: Heightened amygdala reactivity and event-related responses to positive social stimuli in Williams syndrome. *J Neurosci* 29:1132–1139.
29. Leyfer O, Woodruff-Borden J, Mervis CB (2009) Anxiety disorders in children with williams syndrome, their mothers, and their siblings: Implications for the etiology of anxiety disorders. *J Neurodev Disord* 1:4–14.
30. Muñoz KE, et al. (2010) Abnormalities in neural processing of emotional stimuli in Williams syndrome vary according to social vs. non-social content. *Neuroimage* 50:340–346.
31. Medford N, Critchley HD (2010) Conjoint activity of anterior insular and anterior cingulate cortex: Awareness and response. *Brain Struct Funct* 214:535–549.
32. Mesulam MM, Mufson EJ (1982a) Insula of the old world monkey. I. Architectonics in the insulo-orbito-temporal component of the paralimbic brain. *J Comp Neurol* 212:1–22.
33. Mesulam MM, Mufson EJ (1982b) Insula of the old world monkey. III: Efferent cortical output and comments on function. *J Comp Neurol* 212:38–52.
34. Augustine JR (1996) Circuitry and functional aspects of the insular lobe in primates including humans. *Brain Res Brain Res Rev* 22:229–244.
35. Allman JM, et al. (2010) The von Economo neurons in frontoinsular and anterior cingulate cortex in great apes and humans. *Brain Struct Funct* 214:495–517.
36. Seeley WW, et al. (2007) Dissociable intrinsic connectivity networks for salience processing and executive control. *J Neurosci* 27:2349–2356.
37. Nimchinsky EA, et al. (1999) A neuronal morphologic type unique to humans and great apes. *Proc Natl Acad Sci USA* 96:5268–5273.
38. Sridharan D, Levitin DJ, Menon V (2008) A critical role for the right fronto-insular cortex in switching between central-executive and default-mode networks. *Proc Natl Acad Sci USA* 105:12569–12574.
39. Cohen JD, et al. (2010) Morphometry of human insular cortex and insular volume reduction in Williams syndrome. *J Psychiatr Res* 44:81–89.
40. Olsen RK, et al. (2009) Retinotopically defined primary visual cortex in Williams syndrome. *Brain* 132:635–644.
41. Mori S, Zhang J (2006) Principles of diffusion tensor imaging and its applications to basic neuroscience research. *Neuron* 51:527–539.
42. Highley JR, Walker MA, Esiri MM, Crow TJ, Harrison PJ (2002) Asymmetry of the uncinate fasciculus: A post-mortem study of normal subjects and patients with schizophrenia. *Cereb Cortex* 12:1218–1224.
43. Kurth F, Zilles K, Fox PT, Laird AR, Eickhoff SB (2010) A link between the systems: Functional differentiation and integration within the human insula revealed by meta-analysis. *Brain Struct Funct* 214:519–534.
44. Caruana F, Jezzini A, Sbriscia-Fioretti B, Rizzolatti G, Gallese V (2011) Emotional and social behaviors elicited by electrical stimulation of the insula in the macaque monkey. *Curr Biol* 21:1–5.
45. Amodio DM, Frith CD (2006) Meeting of minds: The medial frontal cortex and social cognition. *Nat Rev Neurosci* 7:268–277.
46. Tager-Flusberg H, Sullivan K (2000) A componential view of theory of mind: Evidence from Williams syndrome. *Cognition* 76:59–90.
47. Porter MA, Coltheart M, Langdon R (2008) Theory of mind in Williams syndrome assessed using a nonverbal task. *J Autism Dev Disord* 38:806–814.
48. Karmiloff-Smith A, Kllma E, Bellugi U, Grant J, Baron-Cohen S (1995) Is There a social module? Language, face processing, and theory of mind in individuals with williams syndrome. *J Cogn Neurosci* 7:196–208.
49. Di Martino A, et al. (2009) Functional brain correlates of social and nonsocial processes in autism spectrum disorders: An activation likelihood estimation meta-analysis. *Biol Psychiatry* 65:63–74.
50. Fox MD, Raichle ME (2007) Spontaneous fluctuations in brain activity observed with functional magnetic resonance imaging. *Nat Rev Neurosci* 8:700–711.
51. Mesulam MM (1998) From sensation to cognition. *Brain* 121:1013–1052.
52. Pessoa L (2008) On the relationship between emotion and cognition. *Nat Rev Neurosci* 9:148–158.
53. Damasio AR (1989) Time-locked multiregional retroactivation: A systems-level proposal for the neural substrates of recall and recognition. *Cognition* 33:25–62.
54. Reiss AL, et al. (2004) An experiment of nature: Brain anatomy parallels cognition and behavior in Williams syndrome. *J Neurosci* 24:5009–5015.
55. Karmiloff-Smith A, et al. (2004) Exploring the Williams syndrome face-processing debate: The importance of building developmental trajectories. *J Child Psychol Psychiatry* 45:1258–1274.
56. Karmiloff-Smith A (2009) Nativism versus neuroconstructivism: Rethinking the study of developmental disorders. *Dev Psychol* 45:56–63.
57. Jabbi M, Bastiaansen J, Keysers C (2008) A common anterior insula representation of disgust observation, experience and imagination shows divergent functional connectivity pathways. *PLoS ONE* 3:e2939.
58. Craig AD (2010) The sentient self. *Brain Struct Funct* 214:563–577.
59. Lamm C, Singer T (2010) The role of anterior insular cortex in social emotions. *Brain Struct Funct* 214:579–591.
60. Hamer DH (2002) Genetics. Rethinking behavior genetics. *Science* 298:71–72.
61. Ashburner J (2007) A fast diffeomorphic image registration algorithm. *Neuroimage* 38:95–113.
62. Wakana S, et al. (2007) Reproducibility of quantitative tractography methods applied to cerebral white matter. *Neuroimage* 36:630–644.